Biologically Inspired Optimal Terminal Iterative Learning Control for Walking in a Hybrid Neuroprosthesis

Ryan-David Reyes, Musa Audu, Roger Quinn, Ronald Triolo

***Abstract*— The "Muscle First" Motor-Assisted Hybrid Neuroprosthesis (MAHNP) is a system combining a backdrivable exoskeletal brace with neural stimulation technology to enable persons with paraplegia due to spinal cord injury (SCI) to execute ambulatory motions and to walk upright. The primary purpose of this project is to design a "muscle first" control algorithm to generate ambulatory motion that maximizes activation of the leg muscles to generate the majority of the forces required for walking in the system. This muscle-driven motion is coordinated with the motorized exoskeletal bracing, where the motors inject only the additional power into the system required to ensure that gait motions are completed. In contrast, conventional commercially available exoskeletons cannot efficiently utilize muscle-driven movement due to their non-backdrivable, mechanically inefficient transmissions, and therefore depend on external motors at the joints for all ambulatory motion. In this simulation study, iterative learning control (ILC) maximizes the muscular recruitment with the motorized exoskeletal bracing assisting in a biologically-inspired ballistic fashion. Preliminary data demonstrate the efficacy of the controller in swing-leg simulations created with the OpenSim biomechanical modeling suite and its the ability to learn to balance muscular and motor contributions to improve performance and accomplish safe, consistent stepping.**

***Index Terms*— Hybrid, Neuroprosthesis, Optimal, Terminal, Iterative, Learning, Control, Ballistic**

I. Introduction

RESTORATION of walking is a high priority for persons with paraplegia due to SCI, with one solution being rehabilitative exoskeletons [1]. The commercially available robotic exoskeletal walking assistive devices currently on the market are the Rex, ReWalk, Ekso, and Indego systems [2].

These exoskeletons generate ambulatory motions with mechanical actuators mounted on external bracing worn on the user, or pilot's body. They place the pilot in an upright position as opposed to sitting in a wheelchair, which brings health benefits such as better bowel and bladder function and a reduction in spasticity [3]. However, commercial systems do not activate the paralyzed lower extremity muscles to contribute to walking motions, leaving the lower limbs to continue to atrophy as the actuators are solely responsible for the motive power.

Hybrid exoskeletons, or hybrid neuroprostheses, combine exoskeletal bracing with neuromuscular stimulators to take advantage of biological motive power, with the activation of these muscles mitigating atrophy [4], [5]. These devices use implanted or surface electrodes to deliver the neural stimulation required to recruit the otherwise paralyzed muscles to produce movement coordinated with the active assistance of the exoskeletal bracing.

There are a variety of different methods to efficiently integrate the synergistic forces generated by the lower extremity muscles with the torques generated by the motorized bracing to accomplish ambulatory motion, but certain characteristics of this combined system make coordination difficult. Muscle contractions elicited by neuromuscular stimulation represent highly nonlinear time-varying systems, in contrast to the motorized bracing which is linear time-invariant [4]. Such hybrid systems also exhibit actuator redundancy, with multiple muscles as well as a motor acting on the same joint, allowing a multiplicity of solutions that can generate the same desired joint torque [6].

One of the simplest methods of coordination is to perform trajectory control with the exoskeleton while activating the muscles to reduce control effort and inhibit muscle spasticity during movement [7]. However, this controller does not intelligently allocate control effort between muscle and motor, as the primary aim of the control law is to reduce spasticity.

The switching control method described in [8] has the hybrid neuroprosthesis alternating between two modes to control the knee joints: electrical stimulation only, and motorized bracing only. The controller applies a variable-gain PD controller with delay compensation to the muscles controlling the knee joint, while internally modelling an estimate of the muscle fatigue. Once the estimated fatigue exceeds a pre-specified threshold, the hybrid neuroprosthesis switches to motor control. This approach sidesteps the redundant actuation problem by ensuring that only one set of actuators are active at a time.

Several methods have been proposed that utilize internal models to estimate unobservable states of the system and to distribute control effort across the muscles and motorized bracing. The FEXO Knee, described in [9], controls the muscles with a feedforward controller that incorporates an inverse

muscle model, while applying a PD controller to the motors to enforce a reference trajectory. An optimization algorithm updates the distribution of torque between the knee muscles and the knee motors. This algorithm is designed to keep the contribution from neural stimulation at a fixed amount, and updates only the motor contributions over time. The study described in [10] reports a similar method of control with an inverse muscle model with an extended optimization for joint torque distribution over multiple redundant agonist muscles and actuators, while factoring in an internal estimate of muscle fatigue.

The Exoskeleton Intelligently Communicating and Sensitive to Intention (EICOSI) implements a nonlinear disturbance observer for on-line estimation of generated stimulation torque, which varies the amount of motor assistance based on this estimation [11]. The control method described in [12] incorporates a model predictive controller to generate a desired overall torque, and a second stage which splits the torque contribution between the muscles and motors via a low pass filter. The muscle performs the low-frequency elements of the control signal, with the motor performing the high frequency portions.

There are several studies that augment model predictive control with nonlinear strategies to control hybrid neuroprostheses [13]–[16]. These methods incorporate an optimal predictive controller to determine the best allocation of control inputs across the multiple redundant actuators that act on a single joint, and the nonlinear techniques account for the complex nonlinear dynamics arising from the biological aspects of the system, such as the muscle activation dynamics and electromechanical delay. However, all previously described methods that incorporate an internal model require a sufficiently accurate representation of the system for good performance, as well as a system identification phase to generate model parameters unique to each pilot. The method described in [17] implements model predictive control, but replaces the internal model with a recurrent neural network. This method is computationally complex and would require training the neural network separately to model the capabilities of each pilot.

Iterative learning control (ILC) provides a simple yet robust method for improving the controlled system performance over time. This technique was originally developed for robotics [18], [19], but has since found diverse application in circuit fabrication [20], transportation [21], and even agriculture [22]. It exploits a system that performs repetitive motions and exhibits repetitive errors. ILC algorithms intelligently learn from the errors in the previous iterations to improve performance on the next iteration.

There are several hybrid exoskeleton control methods that treat gait as a repetitive, cyclic system and use ILC inspired methods to achieve coordination between the activated lower limb muscles and the exoskeleton motors. The simplest augments the Indego commercial exoskeleton with stimulation modulated by an ILC algorithm on subsequent steps based on the control effort of the actuators to track a predefined trajectory [23]. Similarly, the Kinesis implements ILC to iteratively update the torque produced by the muscles with the goal of minimizing the interaction torque between the pilot's limb and the device [24]. The ILC in these applications does not modulate motor torque, which is the responsibility of a higher-level controller.

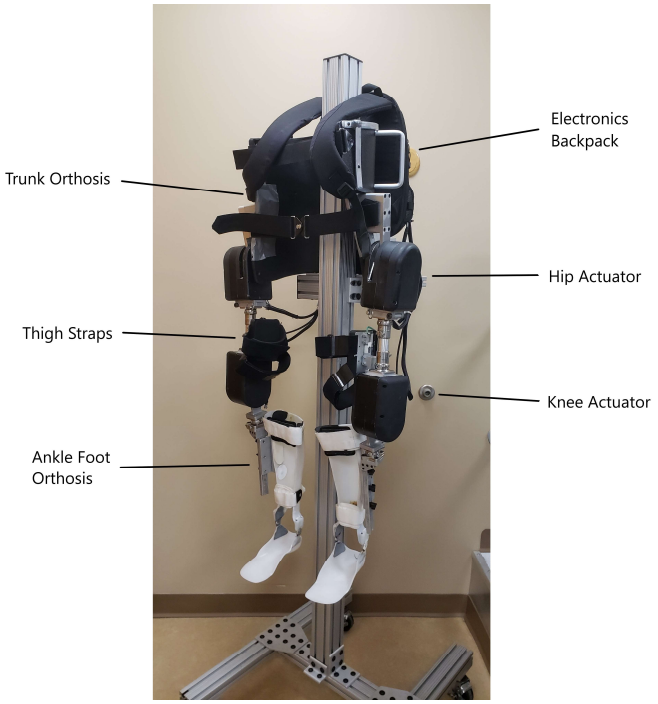

Fig. 1: The "Muscle-First" Motor-Assisted Hybrid Neuroprosthesis.

In [25], the ILC is used to estimate system dynamics to inform a sliding-mode controller. The system then switches between motor or muscle to control the joint depending on an estimate of fatigue. This method is extended in [26], where a neural network based ILC is applied to learn the system dynamics, but requires an additional model predictive controller to allocate control effort between the redundant actuators.

In this simulation study we present the Motor Assisted Hybrid Neuroprosthesis (MAHNP) [27], [28], which combines neuromuscular stimulation with exoskeletal bracing that has backdrivable hip and knee joints with Harmonic Drive Transmissions (Harmonic Drive, Peabody, MA), a complete redesign of our previous passive-hydraulic hybrid neuroprosthesis [29], [30]. To control and coordinate the muscles and actuators of the MAHNP, we propose a Biologically Inspired Optimal Terminal Iterative Learning Control (BIOTILC) algorithm which is a model-free optimal control method derived from [31] which improves its control performance over time, requires no prior system identification, and is able to dynamically and simultaneously allocate torque across the muscles and exoskeletal actuators over each step. A secondary optimization objective is to maximize muscle recruitment, and therefore the physiological benefits of exercise, with the motors assisting-as-needed to achieve a biologically-inspired ballistic swing limb motion.

II. Methods

A. Device and Simulation Design

The MAHNP has four motorized joints: two hip joints and two knee joints (Figure 1). Each actuator weighs 4.85 lbs., is capable of a peak torque of 36 Nm, and requires less than 6 Nm at all joint speeds (0 to 220°/s) for the limb to overcome its passive resistance and backdrive the joint [27], [28]. The actuator is capable of injecting power according to a feedforward model to overcome the internal viscous damping, making the joints act as if nearly frictionless, allowing the contracting muscle to drive the system with the brace retaining the ability to assist-as-needed [27]. Solenoid mechanisms (Thomson Linear, Redford, VA) lock all joints during quiet standing or solely the knee joint during single stance to allow the muscles to rest. The exoskeleton records its internal state, including joint kinematics, and broadcasts this data wirelessly to be stored on a client smartphone or laptop.

The electronics are mounted in a backpack and interface with a neuromuscular stimulator controller board. This board connects with any combination of two 4 channel surface stimulation boards, 12 channel percutaneous boards, or radio frequency boards to control 12 or 16 channel implantable stimulator telemeters [32]. The hip actuators are connected to a fitted, reinforced thoracic-lumbo-sacral orthotic corset, molded to the pilot. The lower extremities are secured in place with straps along the thigh, and the system is connected to the shank via a molded ankle-foot-orthosis that prevents ankle plantar and dorsiflexion and subtalar motion.

A simulation of the biological and mechanical subsystems was developed using the OpenSim musculoskeletal modeling software suite (National Center for Simulation in Rehabilitation Research/Musculographics, Inc.). The simulation is comprised of a single leg in the swing phase connected to a pelvis fixed in space. The biological aspect of the simulation includes an anatomically accurate lower extremity skeleton and contains all relevant muscle groups that are routinely accessible to stimulation in our subjects. The physiological parameters are based on a subject specific model that reflects one of our pilots who has a T4 motor and sensory complete injury. The muscles typically available for stimulation in our system, and for this pilot in particular, are the rectus femoris, vastus lateralis and intermedius, gracilis, sartorius, and tensor fascia latae. The simulation incorporates the relevant masses, inertia, viscous damping, friction compensation, and torque generation characteristics and limitations of the exoskeletal bracing, details of which can be found in Table 1 [28]. The simulated system is illustrated in Figure 2.

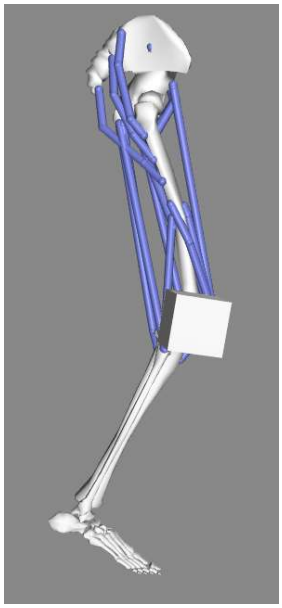

Fig. 2: Swing leg simulation developed in the OpenSim musculoskeletal modeling software. The knee joint actuator is represented by the cube at the knee.

TABLE I
SIMULATED MAHNP CHARACTERISTICS

Characteristic	Quantity	Description
Actuator Masses	2.2 kg	
Actuator Torque Limits	$\pm$36 Nm	Peak torque limit
Viscous Damping Model	$\sigma(\omega) \cdot \lvert b\omega + g \rvert$	Results in < 6Nm of torque required to backdrive actuator at joint speeds of ω =0-220°/s [27]
Feedforward Friction Compensation	$a \cdot \sigma\left(\frac{\omega}{\phi}\right) \cdot \lvert b\omega + g \rvert$	Compensator derived in [27]
Actuator Electrical Current Dynamics	$\tau \frac{dc}{dt} + c = s(t)$	c is the current, $s(t)$ is the current setpoint, τ = 0.0025 resulting in a current rise time of 10ms.

B. Controller Design

To control the pilot's limbs, the MAHNP activates the muscles according to a predefined stimulation pattern, customized to the individual. The muscle activation pattern depends on the strength and availability of the stimulated muscles. Executing this sequence of varying stimulation pulse widths recruits the muscles to produce forces on the joints and results in ambulatory motion.

Human gait is often described as "controlled falling", with the gait patterns naturally taking advantage of passive dynamics to walk in an efficient manner. To begin the swing phase, an impulsive muscle contraction establishes an initial configuration and velocity of the limb. The muscles then relax through rest of swing and the leg completes the motion under the influence of momentum and gravity [33], [34]. The relevant muscle groups are then activated in terminal swing to prepare for weight acceptance. However, unlike able-bodied ambulation, walking with stimulation only [35] or with commercially available powered exoskeletons, does not exhibit this ballistic behavior because of limitations in the strength of the atrophied muscle contractions or the enforced trajectory control by the exoskeletal motors. In our case, powered friction compensation sufficiently reduces the magnitude of viscous damping to allow a short impulse of torque to produce a passive free-swinging motion in the MAHNP under the influence of its own momentum and the force of gravity, much like a two

degree-of-freedom inverted pendulum [28]. This characteristic makes the system amenable to mimicking human gait by programming the motors to produce a burst of flexion torque at the hip and knee for a fixed duration at the beginning of the swing phase to augment the flexor muscles activated via neural stimulation. Once the hip passes a specified flexion threshold, the MAHNP commands a knee extension burst to help complete the step and to ensure that stimulation places the limb into the correct position for weight acceptance.

To enhance this biologically inspired burst control with the ability to improve performance over time and iteratively allocate control effort between the muscles and motors, we explored a BIOTILC approach that modulates the torque bursts and the muscle contributions on each step. Conventional ILC is formulated as a repetitive trajectory tracking problem, with control effort applied throughout the motion providing continuous corrections [19]. In contrast to this, BIOTILC does not impose a trajectory constraint on the MAHNP and only updates the system to enhance the passive portion of swing. The field of Terminal Iterative Learning Control is a formulation of ILC where the main learning objective is controlling the endpoint of the iteration and not maximizing the trajectory performance [20]. This formulation is applied to systems where the start and end points are specified and there is no constraint in how the system traverses between the two points [21]. Additionally, it can be applied to systems where it is impossible to record or estimate the states that occur between the start and the end points [36].

Thus, the learning objective of our system is to ensure that the MAHNP achieves an appropriate lower extremity configuration to accept weight at the end of each step. Additionally, knee flexion must reach a sufficient level during swing to ensure floor clearance. To achieve this learning objective, the controller updates the stimulation as well as the initial motor bursts. The stimulation patterns are augmented with scaling factors applied to the baseline pulse widths generated by the neuromuscular stimulators. The muscles in the pattern corresponding to hip flexion, knee flexion, and knee extension are grouped, and each of these given a corresponding scaling factor. The three scaling factors are α_{hf}, α_{kf}, and α_{ke}, which are the hip and knee flexion and knee extension scaling factors, respectively.

BIOTILC commands three torque impulses to the actuators for a fixed duration: two flexion torque impulses at the hip and knee at the beginning of swing, τ_{hf} and τ_{kf}, and one knee extension torque, τ_{ke}, once the hip has passed a programmed angular threshold. BIOTILC modulates the burst amplitudes of the motors and the scaling factors applied to the relevant part of the stimulation pattern over each step simultaneously. Each swing phase is considered an iteration, with the goal of achieving a desired angular configuration $y_d = \left[y_{hfd}, y_{kfd}, y_{ked}\right]^T$ at a specified time t_f. The terminal error is defined as the deviation of the desired values y_d from actual values y at terminal time t_f.

To account for the redundant actuators of the system, the iterative learning control law is formulated as an optimal control problem [37]. Based on Data-Driven Optimal Terminal Iterative Learning Control (DDOTILC), detailed in [31], a terminal cost function is specified that penalizes terminal error at time t_f and the rate of change of the input $u_k = \left[\tau_{hf}, \tau_{kf}, \tau_{ke}, \alpha_{hf}, \alpha_{kf}, \alpha_{ke}\right]^T$ over each iteration, with k being the iteration index. BIOTILC adds two novel LASSO terms [38] to this cost function to ensure the "muscle first" philosophy - the first of which minimizes the control effort of the motors, the second of which maximizes the recruitment of the muscle.

$$J(u_k) = \left|\left|e_k\right|\right|^2 + \lambda\left|\left|u_k - u_{k-1}\right|\right|^2 + \gamma|x_{mot} \cdot u_k| + \frac{\beta}{|x_{mus} \cdot u_k|} \quad (1)$$

$e_k = y_d - y$ is the terminal error at the end of iteration k. λ is a weighting factor that limits the magnitude of change of u_k between iterations. γ is a weighting factor governs minimizing the motor contribution, as opposed to the β term which governs maximizing muscle contribution. The scaling factors α are defined to always be greater than zero to prevent the β term from being undefined. $x_{mot} = [1, 1, 1, 0, 0, 0]^T$ and $x_{mus} = [0, 0, 0, 1, 1, 1]^T$ are vectors which extract the motor and muscle components from u_k respectively.

The optimal control law has an adaptive learning gain that is a function of an estimate of the partial derivatives of the output y with respect to the inputs u_k [31]. This gradient estimate is defined as

$$\Delta\hat{y}_k = \hat{\Phi}_k \Delta u_k \quad (2)$$

$\Delta\hat{y}_k = \hat{y}_k - y_{k-1}$ is the estimate of the change in output relative to change in input $\Delta u_k = u_k - u_{k-1}$. $\hat{\Phi}_k \in \mathbb{R}^{3\times6}$is the online estimate of the gradient. The following cost function was defined to develop an update law to minimize the error between estimated change in outputs $\Delta\hat{y}$ and the actual change in outputs Δy:

$$J(\hat{\Phi}_k) = \left|\left|\Delta y_{k-1} - \hat{\Phi}_k \Delta u_{k-1}\right|\right|^2 + \mu\left|\left|\hat{\Phi}_k - \hat{\Phi}_{k-1}\right|\right|^2 \quad (3)$$

μ is a weighting term that minimizes the rate of change in the iterative estimate. The iterative gradient update law is computed by taking the partial derivative of the cost function with respect to $\hat{\Phi}_k$ setting it to zero. Solving this system for $\hat{\Phi}_k$ results in the update law [31]:

$$\hat{\Phi}_k = \hat{\Phi}_{k-1} + \frac{\eta\left(\Delta y_{k-1} - \hat{\Phi}_{k-1}\Delta u_{k-1}\right)\Delta u_{k-1}^T}{\mu + \left|\left|\Delta u_{k-1}\right|\right|^2} \quad (4)$$

η is a learning gain that dictates how much the estimate changes due to estimation error over each iteration. The terminal cost function is then rewritten to incorporate the estimate $\hat{\Phi}_k$:

$$J(u_k) = \left|\left|e_{k-1} - \hat{\Phi}_k(u_k - u_{k-1})\right|\right|^2 + \lambda\left|\left|u_k - u_{k-1}\right|\right|^2 + \gamma|x_{mot} \cdot u_k| + \frac{\beta}{|x_{mus} \cdot u_k|} \quad (5)$$

The partial derivative of cost function is taken with respect to u_k and set to zero. Solving for u_k results in the optimal terminal iterative learning control law:

$$u_k = u_{k-1} + \frac{\rho\left(\hat{\Psi}_k^T e_{k-1}\right)}{\left|\left|\hat{\Psi}_k\right|\right|^2 + \lambda} - \frac{\gamma x_{mot}\mathrm{sgn}(x_{mot}\cdot u_k)}{2\left(\left|\left|\hat{\Psi}_k\right|\right|^2 + \lambda\right)} + \frac{\beta x_{mus}}{x_{mus}\cdot u_k |x_{mus}\cdot u_k|}\cdot\frac{1}{2\left(\left|\left|\hat{\Psi}_k\right|\right|^2 + \lambda\right)} \quad (6)$$

For the first iteration, an estimate of the gradient $\hat{\Psi}_0$ is required. In practice, only knowledge of the signs of the elements of $\hat{\Psi}_0$ are needed. To ensure that this algorithm can be realized on actual hardware, the noncausal u_k terms in the dot products on the right-hand side of the update law are replaced with u_{k-1} when implemented. Finally, a reset algorithm is defined in [31] that resets $\hat{\Psi}_k$ to $\hat{\Psi}_0$ if the signs of the elements of $\hat{\Psi}_k$ no longer match those of the initial estimate.

III. Simulation Results

The simulation specified a terminal configuration in terms of a desired hip flexion of $y_{hfd} = 30°$ and a desired knee extension of $y_{ked} = 0°$ at time t_f, to ensure an appropriate limb orientation to accept weight. To guarantee floor clearance, the desired maximum knee flexion was $y_{kfd} = 50°$ during swing. The duration of the step was $t_f = 0.5$s, and the stimulation patterns were time compressed accordingly. The flexion torque bursts commanded to the motors lasted for 0.2s from the onset of swing, and the knee extension burst, or late swing burst, lasted for 0.2 seconds. This latter burst was executed once the hip exceeded a specified threshold of 12° of flexion. The following constants: $\rho = 0.6$, $\beta = 0.8$, $\gamma = 0.5$, $\lambda = 0.1$, $\mu = 1$, $\eta = 0.2$, were applied to BIOTILC to derive the results shown.

The value of ρ was derived heuristically by first isolating its effect on the terminal error across iterations by setting the β and γ terms to zero. Then ρ was set to zero and slowly increased, which resulted in increasing terminal error convergence rate. The system exhibited oscillations in the terminal error once ρ was too large, never reaching a stable, minimal error. At that point, ρ was reduced to the last value that had the highest convergence rate while producing a stable, minimal terminal error. β and γ were then tuned to have tangible effects on maximizing muscle recruitment and minimizing motor control effort, while following a similar tuning routine as described above. An additional stop criterion was when these terms caused a constant offset in error due to the system producing less torque than possible. μ, η, and λ are rate-limiting terms to ensure stable estimates of $\hat{\Psi}$ and u_k, and thus were set to default values found in [31]. Further tuning of these latter constants may provide a higher convergence rate, however there is an increased likelihood of poor performance due to incorrect gradient estimates. BIOTILC was initialized with the following gradient estimate:

$$\hat{\Psi}_0 = \begin{bmatrix} 1 & 0 & 0 & 1 & 0 & 0 \\ 0 & 1 & 0 & 0 & -1 & 0 \\ 0 & 0 & 1 & 0 & 0 & 1 \end{bmatrix}$$

This estimate assumes only redundant actuation and no coupling across joints, i.e., it assumes that both the hip motor and the hip flexion scaling factor influence the amount of terminal hip flexion, whereas the hip flexion torque does not affect the amount of knee flexion. However, if there is coupling between the two terms, BIOTILC should determine the existence and magnitude of the coupling term and account for it automatically.

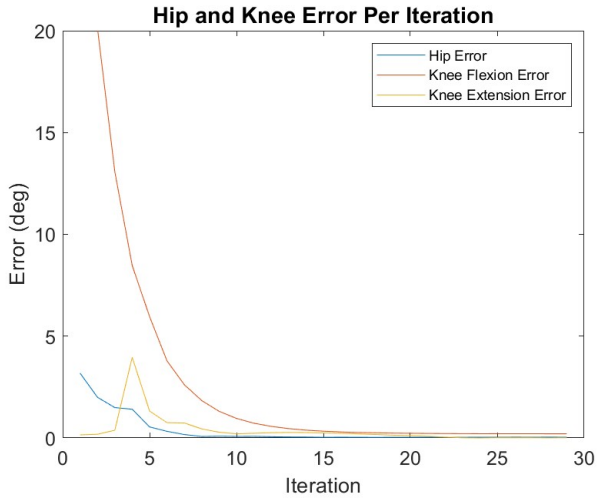

Fig. 4: Absolute terminal error over each iteration for hip and knee flexion, and knee extension.

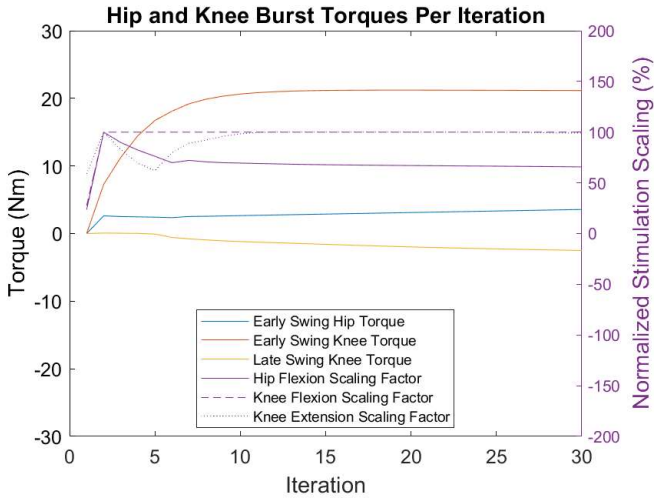

Fig. 4: Muscle and motor recruitment over each iteration. For the left-hand axis, positive values are flexion, negative is extension. Early Swing Torques are executed on the onset of swing. The Late Swing Knee Torque extends the knee to prepare for weight acceptance. The purple lines represent the stimulation scaling factors and are normalized using the scale on the right-hand axis. A scaling of 100% means that the muscles become saturated, i.e., the scaling factor produces a maximized pattern with peak pulse width of 255µs.

The performance of BIOTILC at achieving the learning objective over thirty iterations or steps can be seen in Figure 3. For the first iteration, the motors were commanded zero torque, and all stimulation scaling factors were set to one, meaning that the simulated MAHNP is driven purely by recruited muscle movement via the original stimulation pattern. By the 15th iteration, the system had adapted by maximizing muscular recruitment and assisting as needed with motor bursts to minimize the error. BIOTILC is capable of both ensuring foot

clearance as well as attaining the terminal stance configuration required to accept weight.

After 30 iterations, the estimate $\hat{\Psi}$ was

$$\hat{\Psi}_{30} = \begin{bmatrix} 1.09 & -0.02 & -0.07 & 1.67 & 0.60 & 0.52 \\ -0.07 & 1.69 & -0.02 & 0 & -1.03 & 0.04 \\ -0.01 & 0.07 & 1.05 & -0.05 & -0.05 & 1.01 \end{bmatrix}$$

The algorithm determined that the most significant joint coupling terms were in row 1, columns 5 and 6 of 0.6 and 0.52, respectively. These terms indicate that the change in terminal hip flexion is affected not just by the hip motor (1.09) and hip flexion stimulation scaling factor (1.67), but by an increase in the stimulation scaling factors governing knee flexion (0.60) and knee extension (0.52) as well. One of the muscles recruited for knee flexion was the gracilis, and for knee extension the rectus femoris was activated. Both muscles are biarticular: they affect movement simultaneously across the hip and knee joints. The gracilis contributes to both knee flexion and hip flexion, while the rectus femoris affects both hip flexion and knee extension. It is clear that BIOTILC estimated the coupling terms that indicate the influence of both of these muscles on hip flexion. The entry in row 2, column 2 indicates that the knee flexion motor burst had a large influence on achieving the desired angle for floor clearance. This correlates with the knee flexion burst being the highest commanded torque of all motorized bursts. Finally, there were small, almost negligible estimated coupling influences for the rest of the terms.

The simulations show that we achieved the "muscle-first" objective of maximizing muscle recruitment and minimizing motor control effort, seen in Figure 4. The figure shows the torque commanded to the motors, as indicated by the orange, blue, and yellow lines paired with the left axis. The right axis is paired with the purple lines, which represent normalized stimulation scaling factors. A scaling of 100% means that the multiplicative scaling factor applied to the pattern resulted in the pattern having a peak pulse-width of 255 microseconds, the maximum the stimulator control board can output. The stimulation scaling factor for knee flexion maximized within the first 5 iterations, and the knee extension scaling factor saturated within 15 iterations. The hip flexion scaling factor maximized within 5 iterations, but on further steps BIOTILC determined that with the hip motor, hip flexors such as the sartorius and tensor fascia latae, gracilis, and rectus femoris acting on the joint, it was unnecessary to maximize hip flexor muscle recruitment to achieve the learning objective. The motors made up for any deficits, with 21.1 Nm of flexion torque required from the knee motor to achieve foot clearance. To achieve the terminal configuration only 3.6 Nm hip flexion torque and 2.5 Nm knee extension torque was required of the motors. None of the motors reached maximal peak torque of 36 Nm, while the stimulation scaling factors sans the hip scaling factor were near maximal.

To test BIOTILC's ability to adapt to muscular fatigue, a simple worst-case fatigue model was applied to the system. For this simulation, the BIOTILC weighting terms were identical to those described above, and the initial inputs u_0 and gradient estimation $\hat{\Psi}_0$ were instantiated with the learned values from the 30th iteration of the of the previous simulations, u_{30} and $\hat{\Psi}_{30}$ respectively. For the first five steps of this simulation, muscle

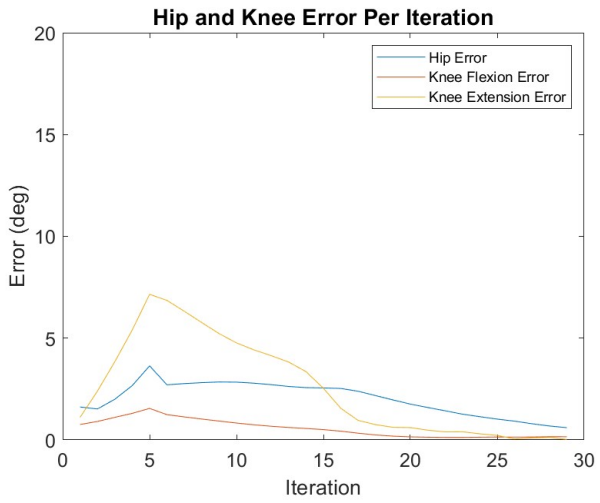

Fig. 65: Absolute terminal error over each iteration in the presence of fatigue.

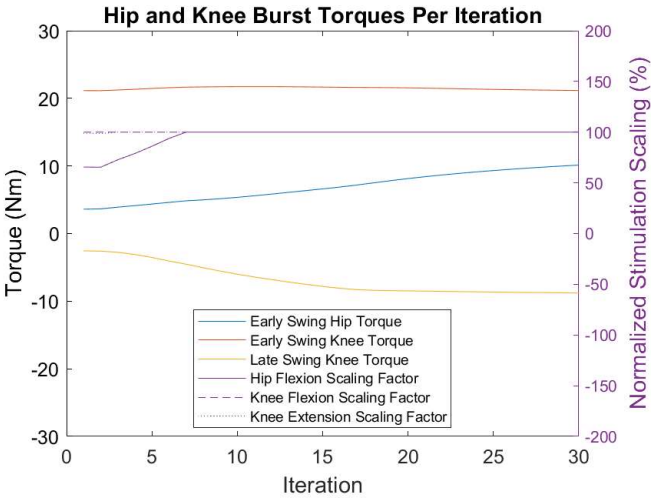

Fig. 6: Muscle and motor recruitment over each iteration in the presence of fatigue. The initial values of muscle and motor recruitment are based on the 30th iteration of the non-fatigue simulation.

torque output decreased by 10%. The system reached 50% strength on the 5th step and remained at that level for all subsequent steps.

Figure 5 depicts the absolute terminal error over each iteration. In the first five steps, the terminal error increased as the muscles weakened. The terminal error peaked at 3.6°, 1.6°, and 7° for the hip flexion, knee flexion, and knee extension errors, respectively. Once the system experienced constant fatigue, BIOTILC adapted, and by the 30th iteration there was less than 0.6° of error for each desired terminal configuration.

Figure 6 shows how control effort is distributed across muscular recruitment and motor burst torques over each iteration. Exhibiting the "muscle-first philosophy", the rate of increase in hip flexion muscular recruitment is faster than the increase in motorized burst torque, becoming maximized at the 7th iteration. Motorized knee flexion torque stayed largely the same, with the motorized hip flexion and knee extension torques reaching 10.12 Nm and 8.8 Nm respectively on the 30th

iteration. These simulations illustrate BIOTILC's ability to adapt to the presence of fatigue in the system.

In the ideal case, the constants derived for this simulation can be transferred to the physical system with little to no changes or further tuning. However, some tuning will be required since the simulation cannot capture all the subtle dynamics of the physical system. Another limitation is that in implementation, the signs of the initial gradient estimate are required, and the several weighting factors must be tuned to ensure convergence and prevent oscillation about the terminal configuration over each iteration.

IV. Conclusion

BIOTILC is a cooperative iterative learning controller designed to control a "muscle-first" motor-assisted hybrid neuroprosthesis that combines neuromuscular stimulation and motorized actuation. It is a model-free algorithm capable of iteratively improving performance by maximizing the recruitment of the muscles and minimizing the motors simultaneously over each step. Simulations of the MAHNP in swing phase show the efficacy of this algorithm in achieving the correct terminal swing configuration, ensuring foot clearance, and exemplifying the "muscle-first" paradigm, as well as adapting to muscular fatigue.

Future avenues for investigation include iteratively learning the stimulation patterns for each muscle over time, as opposed to scaling a pre-existing pattern. Additionally, the algorithm can be extended to control the single stance limb as well as swing limb to drive the system forward. The simulation itself can be enhanced by incorporating the effect of heel strike, as well as removing the fixed constraint on the pelvis and allowing it to move through space to represent natural forward progression of the body.

It has been suggested that an exoskeletal assist-as-needed paradigm requires a forgetting factor applied to the motorized portion of the system to keep the pilot challenged [39]. Thus BIOTILC can be reformulated with a forgetting factor based on an extension of DDOTILC [40]. Additionally, it would be possible to extend the optimal control algorithm with higher order learning terms [41], control of multiple intermediate pass points [42], and initial value dynamic compensation [43]. Finally, efforts are underway to implement BIOTILC on the MAHNP and test the algorithm with SCI pilots.

References and Footnotes

[1] K. D. Anderson, "Targeting recovery: priorities of the spinal cord-injured population," *Journal of neurotrauma*, vol. 21, no. 10, pp. 1371–1383, 2004.

[2] A. D. Gardner, J. Potgieter, and F. K. Noble, "A review of commercially available exoskeletons' capabilities," in *2017 24th International Conference on Mechatronics and Machine Vision in Practice (M2VIP)*, Auckland, Nov. 2017, pp. 1–5, doi: 10.1109/M2VIP.2017.8211470.

[3] L. Miller, A. Zimmermann, and W. Herbert, "Clinical effectiveness and safety of powered exoskeleton-assisted walking in patients with spinal cord injury: systematic review with meta-analysis," *MDER*, p. 455, Mar. 2016, doi: 10.2147/MDER.S103102.

[4] F. Anaya, P. Thangavel, and H. Yu, "Hybrid FES–robotic gait rehabilitation technologies: a review on mechanical design, actuation, and control strategies," *International Journal of Intelligent Robotics and Applications*, vol. 2, no. 1, pp. 1–28, Mar. 2018, doi: 10.1007/s41315-017-0042-6.

[5] A. J. del-Ama, A. D. Koutsou, J. C. Moreno, A. de-los-Reyes, ngel Gil-Agudo, and J. L. Pons, "Review of hybrid exoskeletons to restore gait following spinal cord injury," *The Journal of Rehabilitation Research and Development*, vol. 49, no. 4, p. 497, 2012, doi: 10.1682/JRRD.2011.03.0043.

[6] N. A. Alibeji, V. Molazadeh, B. E. Dicianno, and N. Sharma, "A Control Scheme That Uses Dynamic Postural Synergies to Coordinate a Hybrid Walking Neuroprosthesis: Theory and Experiments," *Frontiers in Neuroscience*, vol. 12, Apr. 2018, doi: 10.3389/fnins.2018.00159.

[7] A. Ekelem and M. Goldfarb, "Supplemental Stimulation Improves Swing Phase Kinematics During Exoskeleton Assisted Gait of SCI Subjects With Severe Muscle Spasticity," *Frontiers in Neuroscience*, vol. 12, Jun. 2018, doi: 10.3389/fnins.2018.00374.

[8] Z. Sheng, V. Molazadeh, and N. Sharma, "Hybrid Dynamical System Model and Robust Control of a Hybrid Neuroprosthesis under Fatigue Based Switching," p. 6, 2018.

[9] D. Zhang, Y. Ren, K. Gui, J. Jia, and W. Xu, "Cooperative Control for A Hybrid Rehabilitation System Combining Functional Electrical Stimulation and Robotic Exoskeleton," *Frontiers in Neuroscience*, vol. 11, Dec. 2017, doi: 10.3389/fnins.2017.00725.

[10] F. Romero-Sánchez, J. Bermejo-García, J. Barrios-Muriel, and F. J. Alonso, "Design of the Cooperative Actuation in Hybrid Orthoses: A Theoretical Approach Based on Muscle Models," *Front. Neurorobot.*, vol. 13, p. 58, Jul. 2019, doi: 10.3389/fnbot.2019.00058.

[11] M. A. Alouane, H. Rifai, K. Kim, Y. Amirat, and S. Mohammed, "Hybrid impedance control of a knee joint orthosis," *Industrial Robot*, vol. 46, no. 2, pp. 192–201, Mar. 2019, doi: 10.1108/IR-08-2018-0165.

[12] H. Vallery, T. Stützle, M. Buss, and D. Abel, "CONTROL OF A HYBRID MOTOR PROSTHESIS FOR THE KNEE JOINT," *IFAC Proceedings Volumes*, vol. 38, no. 1, pp. 76–81, 2005, doi: 10.3182/20050703-6-CZ-1902.01415.

[13] N. A. Alibeji, "A Human Motor Control-Inspired Control System for a Walking Hybrid Neuroprosthesis," Doctoral Dissertation, University Of Pittsburgh, 2017.

[14] N. A. Kirsch, X. Bao, N. A. Alibeji, B. E. Dicianno, and N. Sharma, "Model-Based Dynamic Control Allocation in a Hybrid Neuroprosthesis," *IEEE Transactions on Neural Systems and Rehabilitation Engineering*, vol. 26, no. 1, pp. 224–232, Jan. 2018, doi: 10.1109/TNSRE.2017.2756023.

[15] Xuefeng Bao, N. Kirsch, and N. Sharma, "Dynamic control allocation of a feedback linearized hybrid neuroprosthetic system," in *2016 American Control Conference (ACC)*, Boston, MA, USA, Jul. 2016, pp. 3976–3981, doi: 10.1109/ACC.2016.7525534.

[16] N. Alibeji, N. Kirsch, and N. Sharma, “An adaptive low-dimensional control to compensate for actuator redundancy and FES-induced muscle fatigue in a hybrid neuroprosthesis,” *Control Engineering Practice*, vol. 59, pp. 204–219, Feb. 2017, doi: 10.1016/j.conengprac.2016.07.015.

[17] X. Bao, Z. Sun, and N. Sharma, “A recurrent neural network based MPC for a hybrid neuroprosthesis system,” in *2017 IEEE 56th Annual Conference on Decision and Control (CDC)*, Melbourne, Australia, Dec. 2017, pp. 4715–4720, doi: 10.1109/CDC.2017.8264356.

[18] M. Takegaki and S. Arimoto, “A New Feedback Method for Dynamic Control of Manipulators,” *Journal of Dynamic Systems, Measurement, and Control*, vol. 103, no. 2, pp. 119–125, Jun. 1981, doi: 10.1115/1.3139651.

[19] D. Bristow, M. Tharayil, and A. Alleyne, “A survey of iterative learning control,” *IEEE Control Syst.*, vol. 26, no. 3, pp. 96–114, Jun. 2006, doi: 10.1109/MCS.2006.1636313.

[20] J.-X. Xu, Y. Chen, T. H. Lee, and S. Yamamoto, “Terminal iterative learning control with an application to RTPCVD thickness control&,” p. 8, 1999.

[21] Z. Hou, Y. Wang, C. Yin, and T. Tang, “Terminal iterative learning control based station stop control of a train,” *International Journal of Control*, vol. 84, no. 7, pp. 1263–1274, Jul. 2011, doi: 10.1080/00207179.2011.569030.

[22] S. V. Johansen, M. R. Jensen, B. Chu, J. D. Bendtsen, J. Mogensen, and E. Rogers, “Broiler FCR Optimization Using Norm Optimal Terminal Iterative Learning Control,” *IEEE TRANSACTIONS ON CONTROL SYSTEMS TECHNOLOGY*, p. 13.

[23] K. H. Ha, S. A. Murray, and M. Goldfarb, “An Approach for the Cooperative Control of FES With a Powered Exoskeleton During Level Walking for Persons With Paraplegia,” *IEEE Transactions on Neural Systems and Rehabilitation Engineering*, vol. 24, no. 4, pp. 455–466, Apr. 2016, doi: 10.1109/TNSRE.2015.2421052.

[24] A. J. del-Ama, A. Gil-Agudo, J. L. Pons, and J. C. Moreno, “Hybrid FES-robot cooperative control of ambulatory gait rehabilitation exoskeleton,” *Journal of NeuroEngineering and Rehabilitation*, vol. 11, no. 1, p. 27, 2014, doi: 10.1186/1743-0003-11-27.

[25] V. Molazadeh, Z. Sheng, X. Bao, and N. Sharma, “A Robust Iterative Learning Switching Controller for following Virtual Constraints: Application to a Hybrid Neuroprosthesis,” *IFAC-PapersOnLine*, vol. 51, no. 34, pp. 28–33, 2019, doi: 10.1016/j.ifacol.2019.01.011.

[26] V. Molazadeh, Q. Zhang, and N. Sharma, “NEURAL-NETWORK BASED ITERATIVE LEARNING CONTROL OF A HYBRID EXOSKELETON WITH AN MPC ALLOCATION STRATEGY,” p. 7, 2019.

[27] R.-D. Reyes *et al.*, “Effect of Joint Friction Compensation on a ‘Muscle-First’ Motor-Assisted Hybrid Neuroprosthesis,” *Front. Neurorobot.*, vol. 14, p. 588950, Dec. 2020, doi: 10.3389/fnbot.2020.588950.

[28] M. Nandor, R. Kobetic, M. Audu, R. Triolo, and R. Quinn, “A Muscle-First, Electromechanical Hybrid Gait Restoration System in People with Spinal Cord Injury,” *Front. Robot. AI*, Mar. 2021, doi: 10.3389/frobt.2021.645588.

[29] S. R. Chang, R. Kobetic, and R. J. Triolo, “Effect of exoskeletal joint constraint and passive resistance on metabolic energy expenditure: Implications for walking in paraplegia,” *PLoS ONE*, vol. 12, no. 8, p. e0183125, Aug. 2017, doi: 10.1371/journal.pone.0183125.

[30] S. R. Chang, M. J. Nandor, R. Kobetic, K. M. Foglyano, R. D. Quinn, and R. J. Triolo, “Improving stand-to-sit maneuver for individuals with spinal cord injury,” *Journal of NeuroEngineering and Rehabilitation*, vol. 13, no. 1, Dec. 2016, doi: 10.1186/s12984-016-0137-6.

[31] R. Chi, “Data-driven optimal terminal iterative learning control,” *Journal of Process Control*, p. 12, 2012.

[32] B. Smith *et al.*, “An externally powered, multichannel, implantable stimulator-telemeter for control of paralyzed muscle,” *IEEE TRANSACTIONS ON BIOMEDICAL ENGINEERING*, vol. 45, no. 4, p. 13, 1998.

[33] S. Mochon and T. A. McMahon, “Ballistic walking,” *Journal of Biomechanics*, vol. 13, no. 1, pp. 49–57, Jan. 1980, doi: 10.1016/0021-9290(80)90007-X.

[34] J. Rose and J. G. Gamble, Eds., *Human walking*, 3rd ed. Philadelphia: Lippincott Williams & Wilkins, 2006.

[35] R. Kobetic, R. J. Triolo, and E. B. Marsolais, “Muscle selection and walking performance of multichannel FES systems for ambulation in paraplegia,” *IEEE Trans. Rehab. Eng.*, vol. 5, no. 1, pp. 23–29, Mar. 1997, doi: 10.1109/86.559346.

[36] J. Xu, D. Huang, and W. Wang, “Ballistic learning control: formulation, analysis and convergence,” *J. Control Theory Appl.*, vol. 11, no. 3, pp. 325–335, Aug. 2013, doi: 10.1007/s11768-013-2092-0.

[37] J.-X. Xu and D. Huang, “Iterative Learning in Ballistic Control: Formulation of Spatial Learning Processes for Endpoint Control,” *Journal of Dynamic Systems, Measurement, and Control*, vol. 135, no. 2, p. 024501, Mar. 2013, doi: 10.1115/1.4007236.

[38] R. Tibshirani, “Regression Shrinkage and Selection Via the Lasso,” *Journal of the Royal Statistical Society: Series B (Methodological)*, vol. 58, no. 1, pp. 267–288, Jan. 1996, doi: 10.1111/j.2517-6161.1996.tb02080.x.

[39] J. L. Emken, J. E. Bobrow, and D. J. Reinkensmeyer, “Robotic Movement Training As an Optimization Problem: Designing a Controller That Assists Only As Needed,” in *9th International Conference on Rehabilitation Robotics, 2005. ICORR 2005.*, Chicago, IL, USA, 2005, pp. 307–312, doi: 10.1109/ICORR.2005.1501108.

[40] N. Lin, H. Liang, Y. Lv, and R. Chi, “A forgetting-factor based data-driven optimal terminal iterative learning control with applications to product concentration control of ethanol fermentation processes,” *Transactions of the Institute of Measurement and Control*, vol. 41, no. 14, pp. 3936–3942, Oct. 2019, doi: 10.1177/0142331219841416.

[41] R. Chi, Y. Liu, Z. Hou, and S. Jin, “Data-driven terminal iterative learning control with high-order learning law for a class of non-linear discrete-time multiple-input–multiple output systems,” *IET Control Theory & Applications*, vol. 9, no. 7, pp. 1075–1082, Apr. 2015, doi: 10.1049/iet-cta.2014.0754.

[42] T. D. Son and H.-S. Ahn, “Terminal iterative learning control with multiple intermediate pass points,” in *Proceedings of the 2011 American Control Conference*, San Francisco, CA, Jun. 2011, pp. 3651–3656, doi: 10.1109/ACC.2011.5990633.

[43] R. Chi, B. Huang, D. Wang, R. Zhang, and Y. Feng, “Data-driven optimal terminal iterative learning control with initial value dynamic compensation,” *IET Control Theory & Applications*, vol. 10, no. 12, pp. 1357–1364, Aug. 2016, doi: 10.1049/iet-cta.2015.0824.